

Galaxy formation with radiative and chemical feedback

L. Graziani^{1*}, S. Salvadori², R. Schneider¹, D. Kawata³, M. de Bressan¹, A. Maselli⁴

¹ *INAF Osservatorio Astronomico di Roma, Via Frascati 33, 00040, Monte Porzio Catone (RM), Italy*

² *Kapteyn Astronomical Institute, Landleven 12, NL-9747 AD Groningen, the Netherlands*

³ *Mullard Space Science Laboratory, University College London, Holmbury St. Mary, Dorking, Surrey, RH5 6NT, UK*

⁴ *EVENT Lab for Neuroscience and Technology, Universitat de Barcelona, Passeig de la Vall d'Hebron 171, 08035 Barcelona, Spain*

April 2014

ABSTRACT

Here we introduce **GAMESH**, a novel pipeline which implements self-consistent radiative and chemical feedback in a computational model of galaxy formation. By combining the cosmological chemical-evolution model **GAMETE** with the radiative transfer code **CRASH**, **GAMESH** can post process realistic outputs of a N-body simulation describing the redshift evolution of the forming galaxy. After introducing the **GAMESH** implementation and its features, we apply the code to a low-resolution N-body simulation of the Milky Way formation and we investigate the combined effects of self-consistent radiative and chemical feedback. Many physical properties, which can be directly compared with observations in the Galaxy and its surrounding satellites, are predicted by the code along the merger-tree assembly. The resulting redshift evolution of the Local Group star formation rates, reionisation and metal enrichment along with the predicted Metallicity Distribution Function of halo stars are critically compared with observations. We discuss the merits and limitations of the first release of **GAMESH**, also opening new directions to a full implementation of feedback processes in galaxy formation models by combining semi-analytic and numerical methods.

Key words: Cosmology: theory, galaxies: formation, evolution, stellar content, star formation, Population II, reionisation, radiative feedback, Milky Way

1 INTRODUCTION

Since the pioneering work of Couchman & Rees (1986), the radiative feedback induced by cosmic reionisation has been recognised to have a strong impact on the formation and evolution of galaxies (Gnedin 2000; Benson et al. 2002b,a; Somerville 2002; Hoesft et al. 2006; Okamoto, Gao & Theuns 2008; Salvadori & Ferrara 2009; Lunnan et al. 2012; Sawala et al. 2014), imprinting specific signatures in the observed properties of the Local Universe (Brown et al. 2012).

Semi-analytic models of galaxy formation (SAM) (see e.g. Benson et al. 2002a,b or Somerville 2002) and numerical simulations, both uni-dimensional (Thoul & Weinberg 1996; Kitayama et al. 2000; Dijkstra et al. 2004; Sobacchi & Mesinger 2013) and three-dimensional (see Gnedin 2000; Hoesft et al. 2006; Okamoto, Gao & Theuns 2008 and references therein) have been performed to determine the efficiency of the radiative feedback and the way it affects galactic star formation (SF) by either an extended (*Gradual*) or instant (*Sharp*) process in red-

shift; however a physically motivated prescription is still missing (Noh & McQuinn 2014). Models with a sharp SF suppression after reionisation generally fail to reproduce the present, observed luminosity function and predict an unacceptable gap between the faint and the bright populations, also showing that a redshift dependence in modelling feedback effects is necessary. The value of the critical mass below which galaxies should be strongly affected by photo-ionisation at fixed redshift is also subject to an intense debate: recent numerical studies (Hoesft et al. 2006; Okamoto, Gao & Theuns 2008) find about one order of magnitude lower masses compared to the original calculations (Gnedin 2000), but all the conclusions critically depend on the reliability of the ionising background (UVB) adopted by the SAM.

The effects of an UVB maintaining the Universe reionised can be also considerable on the structure and properties of the Local Group. The tendency of numerical simulations to over-predict the substructures on small scales compared to the observed population, the so called "missing satellite problem" (Moore et al. 1999; Klypin et al. 1999; Boylan-Kolchin, Bullock & Kaplinghat 2012), is often interpreted as inability to reproduce the inefficient or sup-

* E-mail: luca.graziani@oa-roma.inaf.it

pressed star formation acting in the group of local dwarf galaxies, causing small halos to remain "dark", and then invisible to observations (Alvarez et al. 2009; Busha et al. 2010; Ocvirk et al. 2014). Feedback processes have been invoked to justify this failure of the Λ CDM model, both mechanical (Kravtsov, Gnedin & Klypin 2004; D'Onghia et al. 2009, 2010) and radiative (Efstathiou 1992; Gnedin 2000; Benson et al. 2002a; Somerville 2002; Madau et al. 2008; Noh & McQuinn 2014; Milosavljević & Bromm 2014).

A correct determination of the epoch of hydrogen reionisation on the scale of galaxy formation, self-consistently with the SF suppression operated by radiative feedback, could shed some light also on the nature of the ultra-faint dwarfs population found in the Sloan Digital Sky Survey (SDSS, Willman et al. 2005; Belokurov et al. 2006; Zucker et al. 2006b,a). The discovery of these galaxies, roughly doubling the number of known Milky Way (MW) satellites, forced an update of the old models and opened new questions on whether this population is made by pre-reionisation fossils or it is just the lowest-luminosity tail of classical dwarfs. The answer will critically depend, again, on the way the gas ionisation is modelled and on how radiative effects are taken into account.

By using a data-calibrated model for the formation of the MW and its dwarf satellites, which includes the presence of inefficient star-forming mini-halos and a heuristic prescription to account for radiative feedback, Salvadori & Ferrara (2009) have been able to simultaneously reproduce the observed iron-luminosity relation and the Metallicity Distribution Function (MDF) of nearby dwarf galaxies, including the ultra-faint population. The authors argued that ultra-faint dwarf galaxies might represent the fossil relics of a once ubiquitous population of H_2 -cooling mini-halos that formed before reionisation ($z > 8.5$), similarly to what has been found by independent groups (Madau et al. 2008; Kopolov et al. 2009; Bovill & Ricotti 2009; Muñoz et al. 2009; Bovill & Ricotti 2011a,b) and in agreement with a series of more recent studies (Salvadori & Ferrara 2012; Salvadori et al. 2014). In particular, they find that a gradual suppression of the star-formation in increasingly massive (mini-)halos is necessary to match the observed iron-luminosity relation and the MDF of nearby dwarfs. Although this empirical relation is consistent with the minimum mass for SF settled by an advanced semi-analytic treatment of reionisation (Salvadori et al. 2014), the results still rely on the assumptions made on the nature and efficiency of feedback acting on SF halos. A more detailed modelling is certainly required to understand the *local* effects of in-homogeneous radiative feedback, and its impact on the luminosity function of MW satellites.

It should be noted, on the other hand, that the observed luminosity function of MW satellites is certainly not sufficient to fully constrain semi-analytic models as shown, for instance, by alternative approaches (Macciò et al. 2010; Li, De Lucia & Helmi 2010). The observed number and distribution of luminous satellites can be reproduced with accuracy also by assuming a sharp (i.e. instant) reionisation and a strongly mass-dependent star formation efficiency or by invoking other physical processes as supernovae feedback or tidal stripping.

Recent investigations (Alvarez et al. 2009; Busha et al.

2010; Lunnan et al. 2012; Li et al. 2014) try to make an advance in the treatment of the radiative feedback, mainly by relaxing the assumption of a uniform reionisation field (Macciò et al. 2010; Li, De Lucia & Helmi 2010). These studies generally combine the merger-tree histories of advanced N-body simulations (e.g. Springel et al. 2008) with a semi-analytic radiative transfer (see for instance Zahn et al. 2011) describing an in-homogeneous reionisation process. Despite the different approaches, the population of faint satellites is always highly sensitive to the adopted reionisation model.

We finally point out that the observed properties of the MW satellites in the Local Universe (Salvadori & Ferrara 2009; Salvadori et al. 2014) are the result of the global interplay between radiative, mechanical and eventually chemical feedback and a more comprehensive study is necessary to interpret the various observational signatures left during galaxy evolution: the origin and properties of the observed population of metal-poor stars in our galaxy and the low metallicity tail of the MDF.

In this paper we introduce **GAMESH**, a new pipeline integrating the latest release of cosmological radiative transfer code **CRASH** (Graziani, Maselli & Ciardi 2013) with the semi-analytic model of galaxy formation **GAMETE**, powered by a N-body simulation (Salvadori et al. 2010, hereafter SF10). By following the star formation, metal enrichment and photo-ionisation in a self consistent way, **GAMESH** is an ideal tool to study the effects of photo-ionisation and heating in galaxy formation simulations and can address many of the questions discussed above. Into the bargain, the radiative transfer model adopted by **GAMESH** relies on a Monte Carlo scheme and not only naturally accounts for the inhomogeneities of the ionisation process, but also allows a deep investigation of other radiative transfer effects, a self consistent calculation of the gas temperature, and a more accurate description of the stellar populations responsible for the Milky Way environment reionisation.

In the present work the **GAMESH** pipeline will be applied to the Galaxy formation simulation introduced in Scannapieco et al. (2006) and successfully post-processed by the semi-analytic code **GAMETE** (SF10), to derive the properties of the central galaxy and to compare them with the available observations of the Milky Way system. Although the mass resolution of the adopted N-body does not provide a sufficient statistics of mini-halos to study the missing satellite problem, the robust set of results already obtained with the previous semi-analytic approach offers an excellent validation framework for the **GAMESH** pipeline and allows to appreciate the many advantages of the accurate radiative transfer treatment of **CRASH** coupled with the semi-analytic approach of **GAMETE**. A future work, already in place, will focus on high resolution simulations to address all the scientific problems discussed above with the adequate level of detail.

The paper is organised as follows. In Section 2 we describe the **GAMESH** pipeline by briefly introducing its components and by providing details on the feedback implementation. The Milky Way reionisation simulation is introduced in Section 3 and the results discussed in Section 4. Section 5 finally summarises the conclusions of the paper.

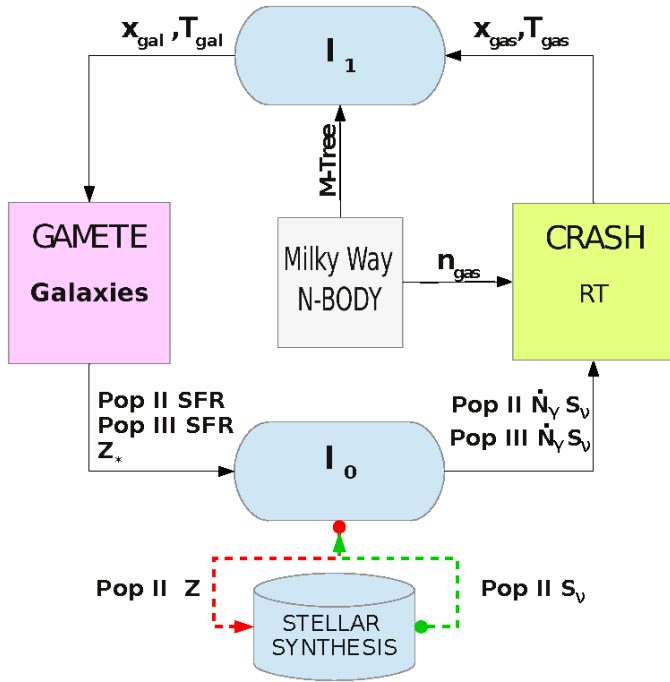


Figure 1. GAMESH pipeline logic at fixed redshift z_i . The quantities x_{gal} , T_{gal} , x_{gas} and T_{gas} refer to the ionisation fractions and temperatures of the gas in the grid cells containing galaxies and in the simulated domain, respectively. The gas number density projected into the grid used by CRASH is indicated as n_{gas} and the global set of information provided by the N-body merger tree as M-Tree. The quantities used by interactor I_0 are the star formation rates (SFR) and the metallicity of the stars (Z_*), while the computed ionisation rates and spectral shapes per galaxy and population are indicated as \dot{N}_γ and S_ν . See text for more details.

2 THE GAMESH PIPELINE

In this section we describe the work-flow of the GAMESH pipeline which integrates a N-body simulation, the semi-analytic code GAMETE (see Section 2.1 for more details), and the radiative transfer code CRASH (see Section 2.2); more details on each pipeline module can be found in dedicated subsections.

GAMESH models the galaxy formation process concatenating a series of snapshots provided by a N-body run at given redshifts $z_{i=0,\dots,N}$: the pipeline uses the physical quantities calculated at z_i as initial conditions for the successive calculation at z_{i+1} . Along the redshift evolution, the feedback between star formation and RT is handled by two software modules called interactors I_0 (detailed in Section 2.3) and I_1 (see Section 2.4). I_0 transforms the galaxy star formation rates (SFR) predicted by GAMETE into a list of ionising sources for CRASH, while I_1 uses the gas ionisation and temperature determined by the RT to establish a star formation prescription for the semi-analytic model implemented in GAMETE. Hereafter we focus on the pipeline logic at fixed z_i (see Figure 1); for an easier reading we also generically refer to the ionisation of the gas as x_{gas} , while a more specific notation will be adopted in Section 4 to discuss the ionisation fractions of hydrogen and helium.

The initial conditions of the pipeline (ICs) are provided by the N-body simulation which assigns the simulation red-

shift z_i to all the components, sets up the N-body merger-tree into I_1 and the gas number density (n_{gas}) in the grid used by CRASH to map the physical domain.

Once the ICs are set up, I_1 starts the simulation by creating a list of galaxies found in the merger-tree: each galaxy is identified by a unique ID and it associates the values of x_{gal} and T_{gal} found in the cell of the grid containing the galaxy center of mass (see section 2.4 for more details). This list is then processed by GAMETE to establish which galaxy can form stars, self-consistently with the metallicity, temperature and ionisation of the accreting gas.

As output of GAMETE we obtain a sub-sample of star forming galaxies, their SFR, stellar metallicity and population type. I_0 converts this sample into a list of CRASH sources by evaluating the galaxy positions on the grid, their spectrum integrated ionisation rate \dot{N}_γ and the spectral shape S_ν . A stellar synthesis database has been implemented in I_0 (see Section 2.3) to derive \dot{N}_γ and S_ν from the stellar metallicity and the SFR.

Once the properties of the radiating galaxies are established, the radiative transfer simulation starts propagating photons for a simulation duration corresponding to the Hubble time separating two snapshots, and it obtains the gas ionisation x_{gas} and temperature T_{gas} at redshift z_i . These quantities are finally used for the subsequent redshift z_{i+1} , by repeating the same algorithm.

Before moving to a more detailed description of the GAMESH components, we want to emphasise the advantages of our approach. We first point out that the use of CRASH allows us to follow with accuracy the process of reionisation of the MW progenitors along the redshift evolution, by taking into account the intrinsic inhomogeneities due to the gas clumps and by calculating the temperature history self-consistently. Moreover, radiative transfer effects, which generally lead to spectral hardening that may preferentially heat gas in overdense regions, will be accounted for by the RT simulation without pre-assuming any propagation model.

The adoption of GAMETE allows us to fully explore the interplay between reionisation, radiative feedback and chemical evolution which can have very interesting and testable consequences (Schneider et al. 2008). Using this approach, we can break the degeneracy between having gradual suppression and constant star formation efficiency or sharp suppression and mass-dependent star formation efficiency.

In the following sections more details on the pipeline components are provided.

2.1 GAMETE

GAMETE (Salvadori, Schneider & Ferrara 2007) is a data-constrained semi-analytic model for the formation of the Milky Way and its dwarf satellites (Salvadori & Ferrara 2009). The algorithm has been designed to study the properties of the first stars and the early chemical enrichment of the Galaxy. The evolution of gas and stars inside each galactic halo of the merger-tree hierarchy (group of Dark Matter (DM) particles) is traced by assuming the following hypotheses:

- the gas is assumed of primordial composition at the highest redshift of the merger tree;

- in each galaxy the SFR is proportional to the cold gas mass;
- the contribution of radiative feedback is accounted for by adopting different prescriptions, depending on the problem at hand. When the code runs in stand-alone mode (i.e. not in pipeline) **GAMETE** assumes instant reionisation (IREion, SF10), i.e. stars form only in galaxies of mass $M_h > M_4(z) = 3 \times 10^8 M_\odot (1+z)^{-3/2}$ ($M_h > M_{30}(z) = 2.89 \times M_4(z)$) prior to (after) reionisation (assumed complete at $z = 6$). When **GAMETE** runs coupled with **CRASH**, star formation is not regulated by the halo mass but by exact radiative feedback effects as predicted by the RT simulation and detailed in Section 2.4. In this case the star formation efficiency in mini-halos (i.e. halos with $T_{vir} < 2 \times 10^4 \text{ K}$) is decreased $\propto T_{vir}^{-3}$ as already detailed in Salvadori & Ferrara (2012), to mimic the effects of a LW background.

Although recent versions of **GAMETE** (Salvadori et al. 2014; de Bennassuti et al. 2014) allow to follow the Pop III / Pop II transition by accounting for detailed chemical feedback (including the dust evolution) and exploring different Pop III IMFs and stellar lifetimes, as well as the effects of the in-homogeneous distribution of metals, the first release of **GAMESH** implements the simplified version of the chemical network as detailed below, for a better comparison with the results in SF10.

- As assumed in the so called ‘critical metallicity scenario’ (Schneider et al. 2002, 2006) low-mass stars form following a standard, Salpeter-like Initial Mass Function (IMF), when the metallicity of the gas is $Z \geq Z_{cr} = 10^{-4} Z_\odot$; when $Z < Z_{cr}$ we assume that Pop III stars form with a mass $m_{\text{Pop III}} = 200 M_\odot$.

- The enrichment of gas within the galaxies and in the diffused MW environment (hereafter Milky Way Environment MWenv) is calculated by including a simple description of supernova (SN) feedback (Salvadori, Ferrara & Schneider 2008). By adopting the Instantaneous Recycling Approximation (Tinsley 1980) we assume that the gas is instantaneously and homogeneously mixed with the atomic metals (see Salvadori, Schneider & Ferrara (2007); Salvadori et al. (2010) for a discussion on the implications of this choice).

The interplay between N-body scheme and semi-analytic calculation, along the redshift evolution of the simulation, is detailed below. At each time-step we distribute the mass of gas, metals and stellar component of each halo among all the DM particles; this is used as ICs of the successive integration step. Metals ejected into the MWenv are treated in the same way so that the newly virialising halos have a chemical composition which depends on the level of enrichment the environment in which they are formed. To recover the spatial distribution of the long-living metal-poor stars at $z = 0$, we also store their properties per DM particle.

2.2 CRASH

CRASH (Ciardi et al. 2001; Maselli, Ferrara & Ciardi 2003; Maselli & Ferrara 2005; Maselli, Ciardi & Kanekar 2009; Graziani, Maselli & Ciardi 2013) is a Monte Carlo based scheme implementing 3D ray tracing of ionising radiation through a gas composed by H and He and atomic metals (e.g. C, O, Si). The code propagates ionising packets with

N_γ photons per frequency along rays crossing an arbitrary gas distribution mapped onto a Cartesian grid of N_c^3 cells. At each cell crossing, **CRASH** evaluates the optical depth τ along the casted path and the amount of absorbed photons $N_{abs} = N_\gamma(1 - e^{-\tau})$. N_{abs} is used to calculate the ionisation fractions of the species $x_{gas} = x_i \in (x_{\text{HII}}, x_{\text{HeII}}, x_{\text{HeIII}})$ and the gas temperature T_{gas} of the crossed cell.

The initial conditions of a **CRASH** simulation are assigned on a three-dimensional Cartesian grid and a cosmological box of linear size L_b , as detailed in the following list:

- the number density of H (n_{H}) and He (n_{He}), the temperature of the gas T_{gas} and the gas ionisation fractions x_i at the initial simulation time t_0^1 ;
- the number of point sources emitting ionising radiation (N_s), their position in the Cartesian grid, their ionisation rate (\dot{N}_γ in photons s^{-1}) and finally their spectral energy distribution (SED, S_ν in $\text{erg s}^{-1} \text{ Hz}^{-1}$). The SED is assigned as an array of frequency bins providing the intensity of the radiation;
- the duration of the simulation (t_f) and a pre-assigned set of simulation times $t_j \in \{t_0, \dots, t_f\}$ used to store the relevant physical quantities;
- the intensity and SED of a UVB, if present.

The interested reader can find more technical information about the latest implementation of **CRASH** and references on its variants in Graziani, Maselli & Ciardi (2013).

2.3 Radiation sources

As explained above, **CRASH** requires the list of all the ionising sources present in the box grid. This is provided in the **GAMESH** framework by the **GAMETE-to-CRASH** module I_0 , responsible of converting the properties of the star forming galaxies (Pop II/Pop III SFR, Z_*) into **CRASH** sources with specific spectral properties.

I_0 first maps the center of mass of each galaxy onto grid coordinates and then converts the star formation rates into spectrum-integrated quantities \dot{N}_γ depending on the stellar population.

For Pop II stars we calculate ionisation rates and spectral shapes accordingly to Bruzual A. & Charlot (1993) and we assume a IMF in the mass range $[0.1 - 100] M_\odot$. A different spectral shape and ionisation rate is then associated with each of the Pop II star forming galaxy depending on its population lifetimes t_* and stellar metallicity Z_* . The spectrum and ionisation rate is derived from a grid of pre-computed spectra integrated in specific lifetime bins $t_* \in \{0.001, 0.01, 0.1, 0.4, 1.0, 4.0, 13.0\}$ Gyr and stellar metallicity $Z_* \in \{0.005, 0.2, 0.4, 1.0, 2.5\} Z_\odot$.

For Pop III stars we assume an ionisation rate per solar mass, $\dot{N}_\gamma = 1.312 \cdot 10^{48}$ [photons s^{-1} / M_\odot] (Schaerer 2002) corresponding to a stellar mass $M_* \sim 200 M_\odot$, averaged on a lifetime of about 2.2 Myr. The SED of Pop III stars is simply assumed as black body spectrum at temperature $T_{BB} = 10^5 \text{ K}$.

¹ n_{gas} is calculated by projecting the particle distribution of the simulation on a Cartesian grid of N_c^3 cells and by deriving the gas component via the universal baryon fraction.

2.4 Radiative feedback

The radiative feedback on the star formation is implemented by the pipeline module I_1 . This module is responsible for setting up the ionisation and temperature ($x_{\text{gal}}, T_{\text{gal}}$) of the gas in the galaxies, successively processed by **GAMETE** to establish their star formation.

At the first redshift z_0 it is simply assumed that the medium is fully neutral (i.e. $x_{\text{gal}} = 0$) and $T_{\text{gal}} = T_0(1 + z_0)$, where T_0 is the value of the CMB temperature at $z = 0$. During the redshift iterations I_1 computes $x_{\text{gal}}, T_{\text{gal}}$ by first finding the cell containing the galaxy center of mass in the **CRASH** grid. As second step, it evaluates which of the surrounding cells best describe the environment from which the galaxy can get the gas to fuel star formation.

The effective environment scale from which cold gas is fuelled into star forming galaxies is crucial to calculate the values of $x_{\text{gal}}, T_{\text{gal}}$ and to apply the radiative feedback. As in our pipeline the gas distribution surrounding halos relies on the spatial resolution of the RT (i.e. the cell size in **CRASH**: $\Delta L = L_b/N_c$), we compare the virial radius R_{vir} of the galactic halo with $\Delta L/2$. We simply assume that if $2R_{\text{vir}}/\Delta L \leq 0.1$, the galactic environment is mainly set up in the cell containing its center of mass and we assign $x_{\text{gal}} = x_{\text{cell}}, T_{\text{gal}} = T_{\text{cell}}$. When, on the other hand, $2R_{\text{vir}}/\Delta L > 0.1$ the gas reservoir of the galaxy could extend to the surrounding cells and then T_{gal} is assigned to their volume averaged value; the value of x_{gal} remains instead the one taken from the central cell. It should be noted though, that the threshold value 0.1 depends on the resolution of the **CRASH** grid and must be tuned for increased resolutions grids, when necessary ².

Once the temperature and ionisation fractions affecting the galactic star formation have been assigned, we first use x_{gal} to evaluate the mean molecular weight μ of the gas and then to calculate the virial temperature of the galactic halo T_{vir} (see the formulas in Barkana & Loeb 2001).

Star formation in the galaxy is finally admitted in **GAMETE** if the condition $T_{\text{gal}} < T_{\text{vir}}$ applies, allowing accretion of cold gas in the galaxy to form stars. In the next version of **GAMESH** we will refine the star formation prescription also accounting for gas cooling, metallicity dependence and dynamical time scales following the approach described in Noh & McQuinn (2014); also see the Introduction for more references and details.

3 MILKY WAY REIONISATION SIMULATION

Here we describe the set-up of our Milky Way reionisation simulation. After a brief description of the N-body simulation and its parameters we detail the radiative transfer assumptions and the initial conditions.

Following Scannapieco et al. (2006), we adopt a cold dark matter (Λ CDM) cosmological model with $h = 0.71$,

$\Omega_0 h^2 = 0.135$, $\Omega_\Lambda = 1 - \Omega_0$, $\Omega_b h^2 = 0.0224$, $n = 1$ and $\sigma_8 = 0.9$.

3.1 The N-body simulation

To study the Milky Way reionisation we adopt the snapshots and merger tree from a cosmological N-body simulation of the Milky Way-sized galaxy halo carried with **GCD+** (Kawata & Gibson 2003a), which were used in Scannapieco et al. (2006). The detail of the simulation is described in Scannapieco et al. (2006); here we briefly summarise the simulation parameters necessary to understand the global **GAMESH** run.

The mass adopted for the N-body particles is $M_p = 7.8 \cdot 10^5 M_\odot$ and the softening length used is 540 pc. The simulated system consists of about 10^6 particles within the virial radius $R_{\text{vir}} = 239$ kpc for a total virial mass $M_{\text{vir}} = 7.7 \cdot 10^{11} M_\odot$. Note that the virial mass and virial radius estimated by observations for the Milky Way are $M_{\text{vir}} = 10^{12} M_\odot$ and $R_{\text{vir}} = 258$ kpc respectively (Battaglia et al. 2005).

Using a multi-resolution technique (Kawata & Gibson 2003b), the initial conditions at $z = 56$ are set up to resolve the region in a sphere within the radius of $R = 4R_{\text{vir}}$ with the high-resolution N-body particles of mass $M_p = 7.8 \cdot 10^5 M_\odot$ and with the softening length of 540 pc; the other region is resolved instead with lower resolution particles.

The simulation snapshots are provided with regular intervals every 22 Myr between $z = 8$ and 17 and every 110 Myr for $z < 8$. The virialised DM halos are then identified by friend-of-friend group finder by assuming a linking parameter $b = 0.15$ and a threshold number of particles of 50; the resulting minimum mass halo is $M_h = 3.75 \times 10^7 M_\odot$.

A validating N-body simulation at lower resolution, also including a star formation recipe, has also been performed to confirm that the assumed initial condition lead to a disc formation (see Brook et al. 2007).

3.2 The RT set-up

The radiative transfer simulation is performed at each redshift z_i , on a box size of $2h^{-1}$ Mpc comoving, by emitting $N_p = 10^6$ photon packets from each star-forming galaxy³. The box is mapped on a Cartesian grid of $N_c = 128$ cells per cube side, providing a cell resolution of $\Delta L \sim 15.6h^{-1}$ kpc. The gas in the box is assumed of cosmological composition (92% H and 8% He) and we neglect the metal ions and the effects of the metal cooling around the star-forming halos. We defer to a future application the extension of **GAMESH** to the metal ions. For a gas of cosmological composition ($n_{\text{HI}} \sim 92\% n_{\text{gas}}$) the ionising spectrum is usually assigned in the energy range $13.6 \text{ eV} \leq E_\gamma \leq 140 \text{ eV}$. Note that the spectral database could be extended at any time to include harder spectra accounting for sources emitting higher energy photons. Note also that the **CRASH** calculation adopts the same cosmological parameters as in the N-body simulation to maintain consistency across the pipeline life-cycle.

² Improving the accuracy of the galactic environment description would ideally require to selectively resolve the halo structures (i.e. a cell size $\Delta L \ll R_{\text{vir}}$), as obtained by using cell refinements around the galaxies. The spatial resolution adopted in the paper simulation is documented in Section 3.2

³ Note that according to the pipeline algorithm each source could have a 'a priori' different spectrum assigned by I_0 as function of its lifetime and stellar metallicity.

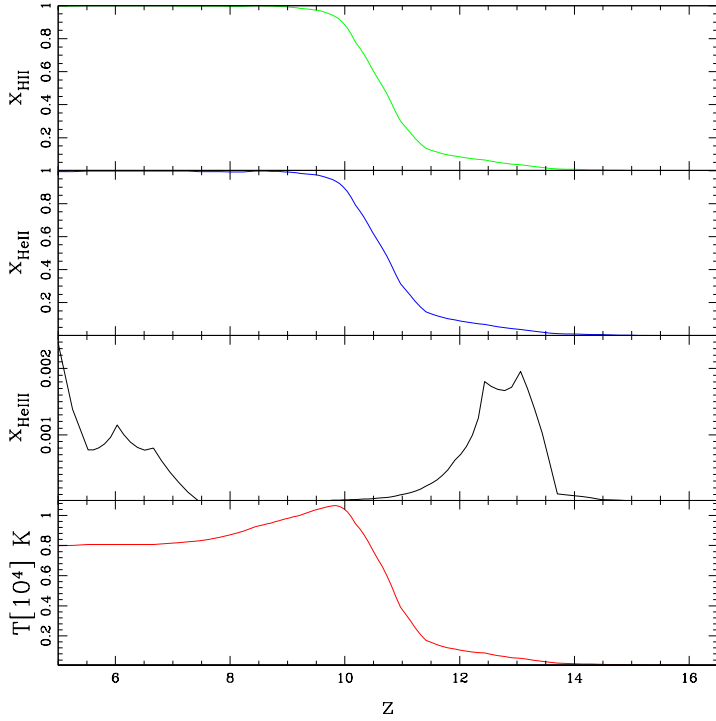


Figure 2. Redshift evolution of the volume averaged ionisation fractions and temperature of the gas, down to $z \sim 5$. From top to bottom the values of x_{HII} , x_{HeII} , x_{HeIII} , $T[10^4]$ K are shown in solid green, blue, black and red lines respectively.

The convergence of the Monte Carlo sampling is guaranteed by an identical run with a factor of ten larger N_p and providing the same numbers within the fourth decimal of the volume average ionisation and temperature created in the box.

The simulation starts at $z_0 \sim 16^4$ with uniform temperature $T_0 \sim 46$ K and we assume that the reionisation is completed when the volume-averaged ionisation fraction of the hydrogen reaches the value $x_{\text{HII}} \geq 0.995$ against the gas recombination. Due to the large excursion in Hubble time, a gas recombination CASE-B is adopted in the simulation and the diffuse re-emission is neglected.

In the absence of a model for the UV background on the scale of the MW formation, we avoid using an external cosmological UVB as done in other works present in the literature, and prefer to mimic a flux entering our box by applying periodic boundary conditions to the escaping radiation. While this choice guarantees that the photon mean free path is conserved when the box ionisation is advanced and the gas becomes transparent to the hydrogen-ionising radiation, it should be noted that we do not account for an external ionising flux likely emitted by the background of QSO sources established below $z \sim 4$.

4 RESULTS

In this section we discuss the results of our simulation, also comparing them with trends obtained adopting the assumption of instant reionisation at $z \sim 6$ as discussed in SF10. Hereafter, for an easier reading, we omit the label "gas" in the variable names referring to ionisation fractions and temperature of the gas and we comment on the single ionised species $x_i \in (x_{\text{HII}}, x_{\text{HeII}}, x_{\text{HeIII}})$.

4.1 Reionisation and temperature histories

Here we investigate the evolution in redshift of the volume averaged ionisation fractions and temperature (in this section $x_i(z), T(z)$) resulting from the radiative transfer simulation.

In Figure 2 we show the redshift evolution of x_{HII} (top panel) and $x_{\text{HeII}}, x_{\text{HeIII}}$ (second and third panels from top) down to $z = 5^5$. x_{HII} remains below $x_{\text{HII}} \sim 0.1$ when $z > 12$, afterwards it rapidly rises up to $x_{\text{HII}} \sim 0.5$ at $z \sim 11$ and reaches $x_{\text{HII}} \sim 0.9$ when $z \sim 10$. The sudden increase in the hydrogen ionisation fraction in the redshift range $10 < z \leq 12$ can be ascribed both to the rising in the co-moving SFR (Figure 4) and in the total number of emitting galaxies (Figure 5) but more likely to an advanced stage of overlapping of ionised regions, which makes the reionisation process intrinsically non-linear.

Below $z \sim 10$ the hydrogen reionisation wades through and x_{HII} increases up to 0.99 by $z \sim 9$ and up to 0.999 by $z \sim 5$. Even if not visible in the Figure, we point out that below $z \sim 8.5$ the value of the third decimal of x_{HII} continues to oscillate in $0.997 \leq x_{\text{HII}} \leq 0.999$ due to the continuous unbalance in the gas ionisation, created by the ongoing gas collapse that enhances the recombination rate at the center, and by the in-homogeneous reionisation/recombination occurring in the volume. We consider the hydrogen reionisation completed at $z \sim 6.4$ when $x_{\text{HII}} > 0.995$, neglecting these fluctuations.

The second and third panels from top, show the ionisation histories of helium. It is immediately evident that the HeI reionisation can be sustained only by the Pop II stars dominating below $z \sim 12$ while the reionisation of HeII never occurs at the considered Milky Way scale (here $2h^{-1}$ Mpc comoving) without the contribution of an external background of harder spectra (e.g. QSO). In fact, while the redshift trend of x_{HeII} follows the one of the hydrogen, x_{HeIII} never reaches values higher than $x_{\text{HeIII}} = 0.002$ along the entire redshift range. As also pointed out for x_{HII} , the volume averaged ionisation fraction of HeII continues to oscillate in $0.97 < x_{\text{HeII}} < 0.99$ below $z \sim 8.5$, confirming that a harder spectral component is required to sustain full helium ionisation against gas recombination. Note that a bump in the value of x_{HeIII} (third panel from top) occurs in the redshift range $12 < z < 15$, tracing the presence of Pop III stars (see also Figure 4) with their harder spectral shapes. Note also that the volume averaged value of x_{HeIII} remains always negligible over the entire simulation: after

⁴ This is the first redshift in which the applied FoF is able to identify the first halos. This redshift value depends on mass resolution of the simulation.

⁵ Below this redshift a uniform ionised pattern of hydrogen is created and the values are less indicative. Note that we cannot discuss the helium reionisation due to the absence of a harder radiation background.

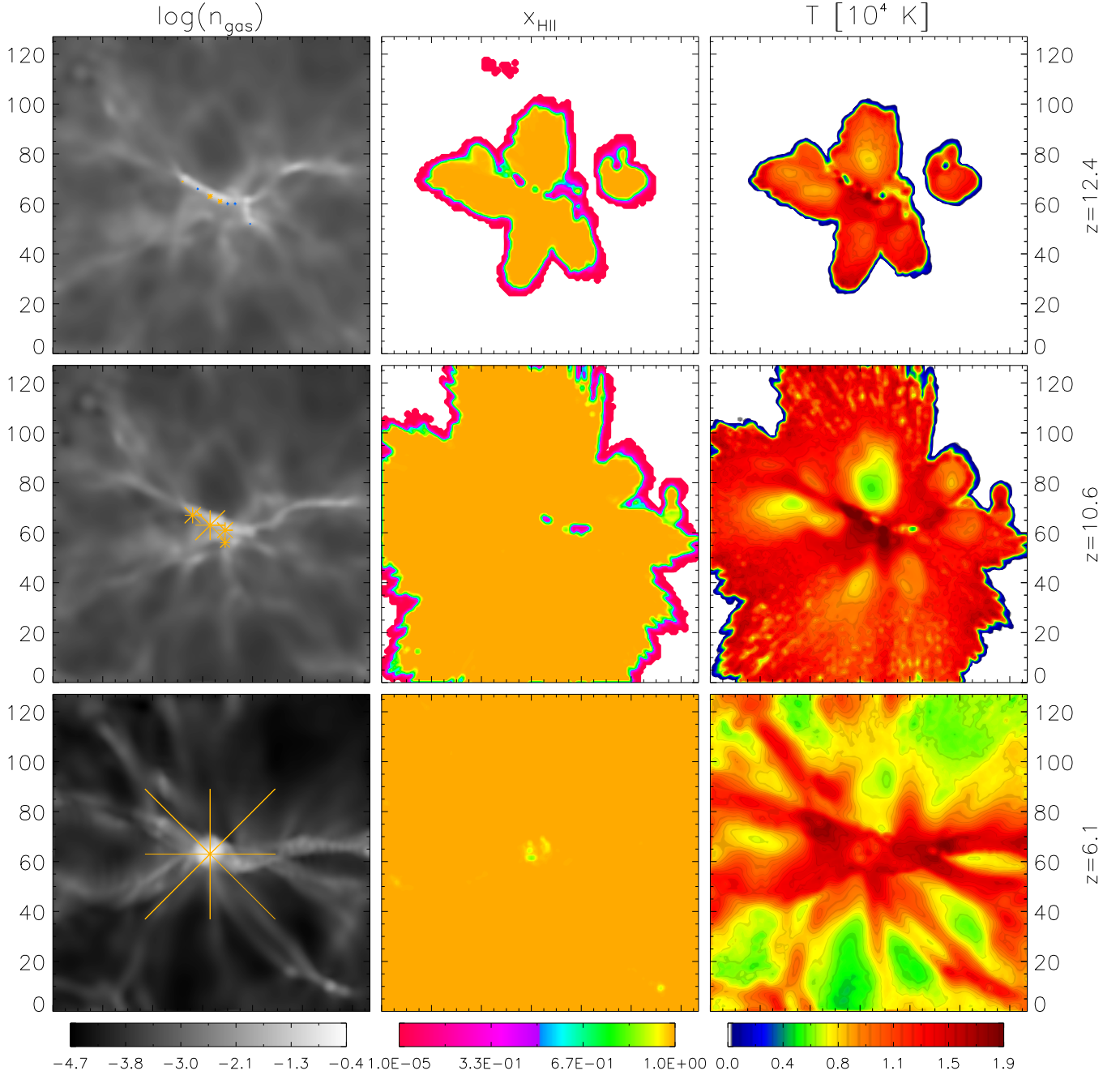


Figure 3. Slice cuts of n_{gas} (first column), x_{HII} (second column), T (third column) at three different redshifts: $z \sim 12$ (top panels), $z \sim 11$ (middle panels), $z \sim 6$ (bottom panels). The value of the fields in the plane are represented as colour palettes and the distance units are expressed in number of grid cells along the x and y axis ($\sim 15.6h^{-1}$ kpc per cell). In the first-column panels star forming galaxies are symbolised as blue crosses when forming Pop III stars, while as gold-yellow asterisks for Pop II stars; the sizes of the symbols are scaled with the galaxy ionisation rate \dot{N}_γ .

the transition from Pop III to Pop II stars the presence of full ionised helium is so closely confined to the sources that is not visible in the panel, except at $z < 7$, when hydrogen ionisation is complete and harder photons ($E_\gamma > 54.4$ eV) are free to cross the box many times and to create a very small ionisation fraction of fully ionised helium.

The redshift evolution of the volume-average temperature is shown in the bottom panel of Figure 2 in $[10^4 \text{ K}]$ scale. Before $z \sim 10$, the temperature rises from the initial value $T \sim 50 \text{ K}$ up to $T \sim 10^4 \text{ K}$; note that the rapid evolution of Pop III stars in this redshift range is so small (not visible in the plot) that it cannot change the global trend of the average temperature. In the redshift interval $9 < z < 10$ the gas stabilises at a average photo-ionisation equilibrium temperature of $T \sim 10^4 \text{ K}$, before its average value starts decreasing by some 10^3 K during the successive evolution. Oscillations of the order of 10^3 K are present below $z \sim 5$ (not shown in the plot), due to the competitive effects of gas clumping toward the center, adiabatic cooling due to the cosmological expansion, and finally in-homogeneous distribution and properties of the ionising galaxies. Even if not visible in this plot we report a final average temperature of $T = 7.9 \times 10^3 \text{ K}$ at $z = 0$ but we remind that this value is certainly underestimated in our simulation due to the absence of high energy photons from the QSO background established on the large scale below $z \sim 4$.

To visually illustrate how the reionisation process evolves in space and redshift, we show in Figure 3 three slice cuts of our volume (of $2h^{-1}$ comoving Mpc side length) taken at redshifts $z \sim 12, 11, 6$ (see panels from top to bottom). Panels in the first column show $\log(n_{\text{gas}}(z))$ as gray gradient from black ($n_{\text{gas}} \sim 2 \times 10^{-5} \text{ cm}^{-3}$) to white ($n_{\text{gas}} \sim 0.4 \text{ cm}^{-3}$); in the second column $x_{\text{HII}}(z)$ is shown by a colour palette from violet ($x_{\text{HII}} = 10^{-5}$) to orange ($x_{\text{HII}} = 1.0$), and finally the pattern of $T(z)$ is drawn in the third column with a different colour palette from white ($T \sim 50 \text{ K}$) to dark red ($T \sim 1.9 \cdot 10^4 \text{ K}$). In all the panels, the distances are shown in cell units ($\sim 15.6h^{-1} \text{ kpc}$ per cell) along the x and y directions.

Superposed to the number density maps we also show the star forming galaxies (SFG) present in the surface of choice: galaxies forming Pop III stars are symbolised as blue crosses (top panel), while gold-yellow asterisks are associated with the presence of Pop II stars. Also note that the size of each symbol is scaled with its \dot{N}_γ and the position of star forming galaxies perfectly correlates with the gas filaments, falling toward the center where the central galaxy is progressively forming along the redshift evolution.

As consequence of the central position of the ionising sources, the reionisation proceeds inside-out. At high redshift (top panels), the low density regions surrounding the center of the box (black regions, first column) are easily ionised by the sources (orange pattern, second column). At the center of the image note that high-density clumps (white regions) are able to suppress photo-ionisation with a high gas recombination rate (magenta patterns). The average gas temperature (third column) tends to stabilise around $T \sim 1.4 \times 10^4 \text{ K}$ in the regions involved by the overlap of ionised bubbles (yellow and red), mainly driven by the contribution of Pop III stars. T rapidly decreases down to $T \sim 10^2 \text{ K}$ at the border of the ionised region (blue patterns) not reached by stellar radiation. Consistently with

the ionised pattern, few high-density structures remain self-shielded and settle at very low temperature at the center image. Note that the presence of helium in our simulation significantly changes the gas photo-heating enhancing the contrasts between over-dense regions and voids. At $z \sim 11$ (middle panels) the reionisation process is already quite advanced and the ionising radiation involves a large fraction of the box, including the under-dense regions far away from the center (green and yellow patterns). Voids are rapidly ionised and their temperature stabilises around $T \sim 6 \cdot 10^3 \text{ K}$, well below the central value $T \sim 10^4 \text{ K}$. Finally, at $z \sim 6$ the entire volume reaches photo-ionisation equilibrium and its average temperature stabilises around $T \sim 8.0 \cdot 10^3 \text{ K}$ but the spatial pattern continues to show large variations from the gas filaments (branching off the central MW-type galaxy) and from the under-dense regions.

Note that at the final redshift ($z \sim 6.1$) the central galaxy is seen as single source with highest ionisation rate of about $\dot{N}_\gamma = 2 \cdot 10^{54}$ photons/s and SFR $\sim 13M_\odot/\text{yr}$ (the total SFR of the emitting objects is $\sim 20M_\odot/\text{yr}$). In the other galaxies laying on the plane, the star formation is suppressed by radiative feedback (see Section 4.2.1 for more details)

As final comment, we point out that our simulation lacks the ionising contribution of an external UV background, especially at the helium ionising frequencies. While periodic boundary conditions are adopted to preserve the photon mean free path at all frequencies, the external UVB may play a relevant role because of the small size of the simulation box and its coarse mass resolution. On the other hand, the inclusion of a UVB is neither trivial nor straightforward. First, the available UVB models (see for example Haardt & Madau 2012 and references therein) are computed and calibrated on the large scale structure. Therefore, on the scales of MW formation, both the intensity and the spectral shape of the UVB may be modified by RT effects. By means of the radiation tracking features of CRASH3, we will investigate these effects in a future study. Here we only point out that an external UVB could only impact hydrogen ionisation above $z \sim 11$. In fact, Fig. 2 shows that below this redshift the internal flux is sufficient to sustain hydrogen ionisation.

4.2 Feedback on star formation

The redshift evolution of the comoving SFR is shown in Figure 4, where the red lines refer to the contribution from Pop II stars (highest curve) and the blue lines to Pop III. Dotted lines, with same colours, show the values obtained by adopting the instantaneous reionisation prescription (See Section 2.1). In the redshift interval $12.4 < z \lesssim 16$ the total SFR of our simulation (solid lines) increases up to $1.7M_\odot/\text{yr}$ thanks to both Pop III and Pop II stars, but note that at the highest redshift $z \sim 16.5$ (when the gas is mostly primordial) only population III objects contribute to the total SFR. Feedback from Pop III forming galaxies, both radiative and chemical, acts efficiently on the surrounding medium: their hard spectra locally increase the MWenv temperature inhibiting star formation in unpolluted clouds, while mechanical feedback rapidly pollutes the MWenv up to the critical metallicity $Z_{\text{cr}} = 10^{-4}Z_\odot$. Both effects contribute to their sudden disappearance, triggering the formation of Pop II stars below $z \sim 12.4$. At lower redshift Pop II stars cause an increase of

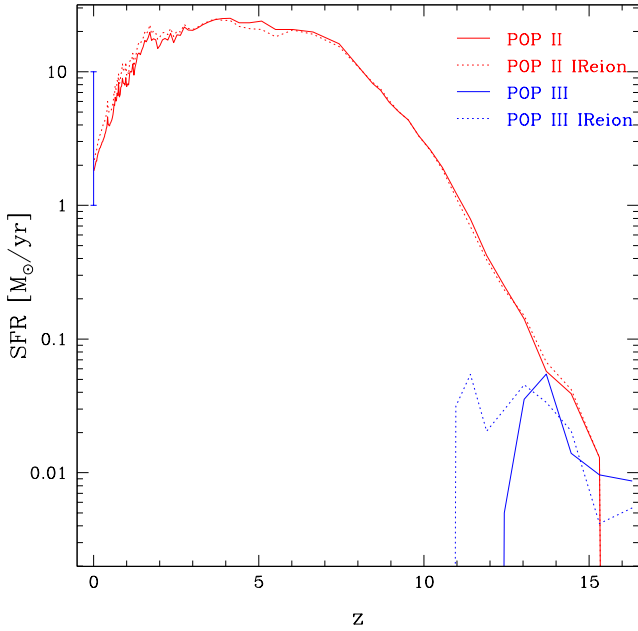


Figure 4. Star formation rate for Pop II (solid red lines) and Pop III (solid blue) as function of z . As reference the values obtained with the instant reionisation approximation (IReion) are shown dotted lines and same colours for the two populations. The value of the SFR estimated by observation at $z = 0$ is reported as error bar. See text for more details.

the total SFR up to a value of $\text{SFR} \sim 25 M_{\odot}/\text{yr}$ at the peak redshift $z \sim 4$. The successive evolution proceeds with an irregular but progressive decrease down to a value of $\text{SFR} \sim 1.8 M_{\odot}/\text{yr}$ at $z = 0$, in good agreement with the observed data (Chomiuk & Povich 2011).

It is interesting to compare these results with the ones obtained with the instant reionisation (IReion) approximation for both populations. We remind that in IReion approximation **GAMETE** accounts for feedback by assuming that only Lyman- α halos having $M_h > M_4$ can form stars at $z > 6$, while at $z \sim 6$ the volume is suddenly ionised and a different threshold applies. For $z < 6$ only halos with circular velocity greater than 30 km s^{-1} (i.e. $M_h > M_{30}$) can trigger the star-formation (see SF10).

By comparing the solid and dotted lines in Figure 4 we immediately conclude that the suppression of star formation operated by the IReion is quite appropriated to reproduce the SFR of Pop II stars in a wide redshift range but it overestimates the SFR at $z = 0$ by 15%. Note also that the stronger radiative feedback effects at high redshift in IReion lower the SFR of Pop III stars and delay the transition between the two stellar populations.

4.2.1 Feedback statistics

The effects of the radiative feedback on the statistics of star forming galaxies are shown in Figure 5 as function of redshift z . The solid blue line indicates the number of SFG computed in our simulation, while the dotted red line refers to the IReion case. The total number of DM halos found in the N-body simulation in use is shown as dashed black line.

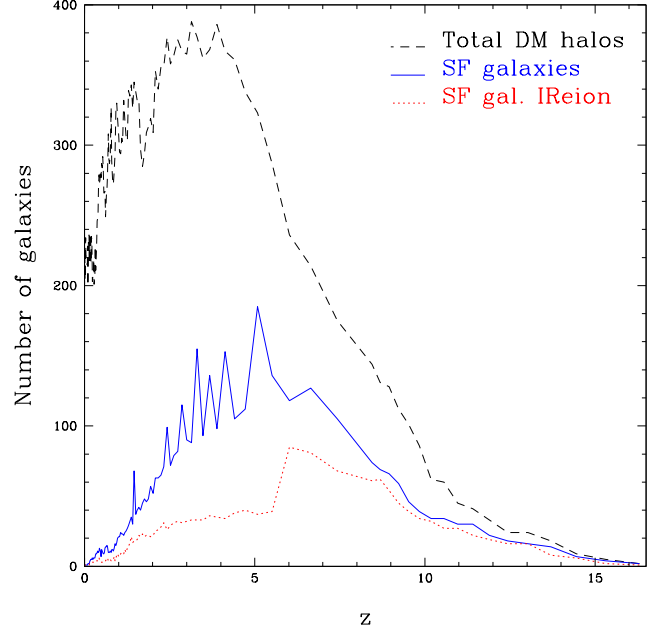


Figure 5. Number of star forming galaxies as function of z in the simulation (solid blue line). The dotted red line refers to the IReion case, while the dashed black line shows, as reference, the total number of DM halos found in the N-body simulation.

By comparing solid and dotted lines, we first note that at the current resolution of the simulation, which does not resolve the full range of masses that sample the mini-halos regime, the condition $M_h > M_4$ could appear quite appropriate to reproduce the statistics of the galaxies with suppressed star formation at very high redshifts ($z > 10$). On the other hand, a careful comparison with Figure 4 immediately shows a different star formation rates of Pop III galaxies (compare blue lines in Figure 4).

This discrepancy can be ascribed to a combination of reasons which involve radiative, mechanical, and chemical feedback. Also note that the IReion model cannot account for in-homogeneous feedback on high-redshift low mass objects (which are likely to host Pop III stars) but indiscriminately applies to *all* the galaxies with $M_h > M_4$ present in the volume. At high redshift this assumption is particularly incorrect because the SFG are still quite separated in space and then their radiative feedback acts very selectively, only affecting their surrounding neighbourhoods. See for example how dis-homogeneous is the bubble overlap in the third panels of Figure 3 and how many regions of the simulated volume remain unaffected by photo-heating.

Note that the current mass resolution of the N-body simulation does not allow to draw robust conclusions on the radiative feedback effects at high-redshift. This will be the subject of a future dedicated study (de Bennassuti et al. 2015, in prep.).

At lower redshifts the efficiency of the radiative feedback increases with the progress of reionisation in both models. In the redshift interval $6 < z \lesssim 9$ the **GAMESH** run predicts that around 50% of the galaxies have been affected by radiative feedback and this value increases up to 65% by $z \sim 4$, with a jagged trend due to both oscillations in

the number of potential galaxies (dashed black line) and the in-homogeneous heating in space induced by the RT⁶. Below $z = 4$ the suppression of star formation in small galaxies progresses rapidly allowing few remaining objects in the box to form stars, as observed in the Milky Way environment.

Note the difference in the statistics of SFG below $z \sim 6$ obtained in the IReion approximation. In fact a realistic radiative feedback operates with a more gradual suppression in time, due to the in-homogeneous nature of the bubble overlap in space. In $3 < z < 6$ this difference induces an error in the number of SFG as high as 40% between the two cases (compare solid blue line with dotted red line). On the other hand this statistical discrepancy between models is not reflected in both the total SFR (Figure 4) and the MWenV enrichment (see Figure 8) which are very similar in this redshift range, also indicating that the high-mass galaxies surviving the IReion prescription provide a dominant contribution to these quantities.

Figure 6 visually shows how the in-homogeneous radiative feedback operates in space, by comparing the same slice cuts and redshift sequence commented in Figure 3. Here, on top of the gas number density field we have traced few solid line iso-contours of the gas temperature: $T \sim 100$ K in cyan, $T \sim 4 \times 10^3$ K in blue, $T \sim 10^4$ K in green, $T \sim 1.3 \times 10^4$ K as orange and finally $T \sim 1.5 \times 10^4$ K in dark-red. All the star forming galaxies are symbolised by yellow asterisks, while the galaxies in which star formation has been suppressed by radiative feedback are shown as black filled circles.

By comparing the three panels it is immediately evident how the inhomogeneities in the reionisation process induce large differences in randomly suppressing star formation (left and middle panel) before a UVB is fully established (right panel). At high redshifts few suppressed SFGs (black circles) are trapped in regions with $T \sim 10^4$ K, not necessarily connected with the emitting galaxies. Note for example the galaxy on the right side of the middle panel: even far from the center it is surrounded by gas with high temperature, that likely originates from more complicated three-dimensional effects created by the RT. On the other hand at $z \approx 6$ (right panel) the medium is already pervaded by a quasi-homogeneous UVB and then all the galaxies below a critical mass are easily suppressed in the entire domain. To study if a critical mass for the suppression of SFGs is statistically restored against the non-linearity induced by the RT, we should rely on a higher resolution simulation providing a better statistics for both Lyman- α and H₂-cooling halos, as well as better spatial resolution. With this study we will be able to provide a numerically motivated recipe for semi-analytic models. We then defer this point to the next work (de Benassuti et al. 2015, in prep.) and limit the discussion to this figure, as an illustrative example of how radiative feedback implemented in GAMESH works.

⁶ As commented in the previous paragraph, only with a higher mass and spatial resolution simulation we can fully understand the impact of an in-homogeneous reionisation process on the statistics of SF galaxies

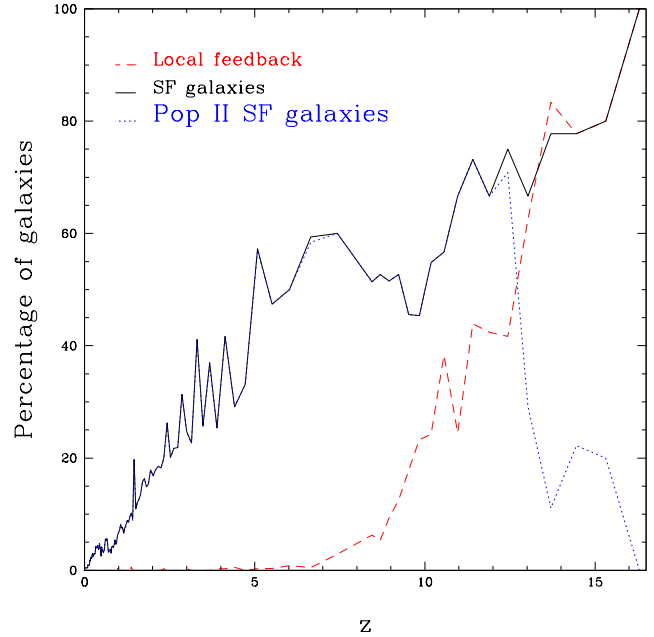


Figure 7. Percentage of star forming galaxies as function of z (solid black line) and percentage of galaxies affected by radiative feedback in their own cell (dashed red line). The blue dotted line shows the percentage of galaxies forming mainly Pop II stars.

4.2.2 Local versus environmental feedback

As introduced in Section 2.4, the radiative feedback defined in GAMESH depends on the spatial extension of the galactic environment feeding cold gas for star formation. Depending on the virial radius of the dark matter halo hosting each galaxy and the spatial resolution of the RT grid, the feedback could act *locally* to the sources (i.e. accounting just for the temperature in the galaxy cell ($2R_{vir} \leq 0.1\Delta L$)) or it could act *globally* involving larger scales (i.e. cells surrounding the one containing the galaxy) when $2R_{vir} > 0.1\Delta L$.

The statistics of these two mechanisms can help to understand the importance of 'local' versus 'global' feedback along the progress of reionisation, establishing a H-ionising uniform UVB. In Figure 7 we show the percentage of SFG (solid black line) together with the percentage of galaxies that are influenced by 'local' feedback (dashed red line)⁷. To understand which stellar population is affected by local or environmental effects we also show in blue dotted line the percentage of galaxies forming Pop II stars.

As already commented in the previous figure, the percentage of SFG (solid black line) rapidly decreases from high to low redshifts following the progress of reionisation with a spiky and irregular trend down to $z \sim 4$. The presence of a "plateau" in the redshift interval $6 < z < 9$ could mark the existence of an extended reionisation epoch in which the gas is kept in photo-ionisation equilibrium in the entire box at $T \sim 10^4$ K and the hydrogen ionisation fraction increases from 0.99 up to 0.999. The dashed line indicates that isolated, high redshift galaxies ($z > 12.4$) are quite insensitive

⁷ These number are calculated with respect to the total number of halos found in the simulation.

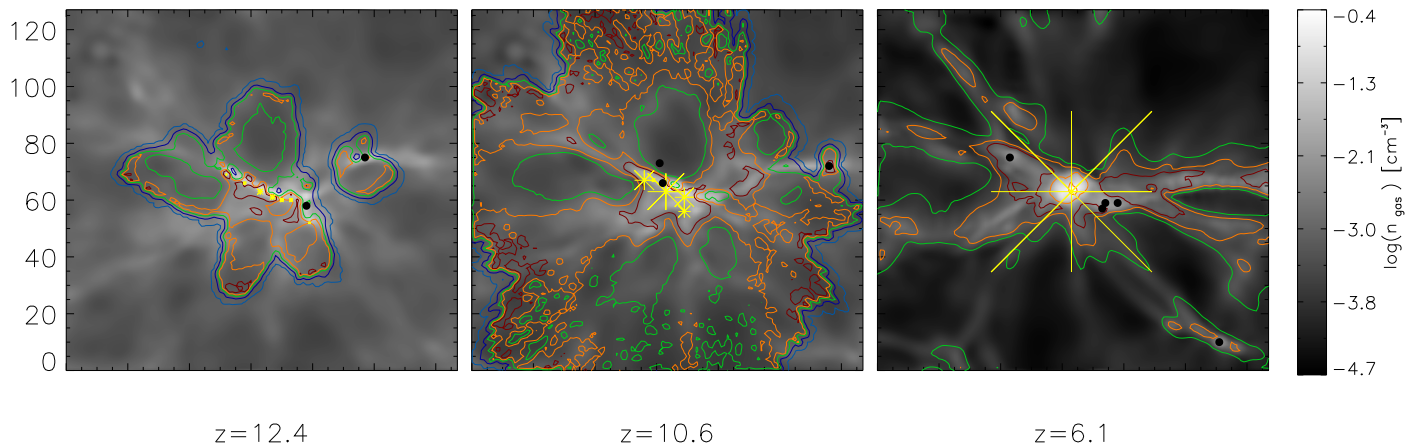


Figure 6. Slice cuts of the gas number density n_{gas} with superposed temperature contour-plots: $T \sim 100$ K (cyan), $T \sim 4 \times 10^3$ K (blue), $T \sim 10^4$ K (green), $T \sim 1.3 \times 10^4$ K (orange) and $T \sim 1.5 \times 10^4$ K in dark-red. All the star forming halos in the plane are represented by yellow asterisks, while black dots indicate halos in the plane in which star formation is suppressed by radiative feedback.

to their environment and the radiative feedback plays only a local role. A quick comparison with the blue dotted line clearly shows that these galaxies mainly form Pop III stars. After the population transition, Pop II forming galaxies are instead progressively affected by their environment: below $z \sim 8$, both the increase of the virial radii of the sources and a more uniform ionising background make the environment progressively more important and the feedback acts globally. At these redshifts the gas temperature is sustained by: i) the few satellite galaxies surviving radiative feedback, ii) the global UVB entering the box, and iii) the predominant emission from the central MW-type Galaxy. It is in fact clear from Figure 7 that less than 40% of galaxies is capable to accrete gas from the surrounding reservoir to fuel the star formation process below $z \sim 4$.

4.3 Interplay with chemical feedback

In this section we briefly investigate how the reionisation process can leave specific signatures in the chemical evolution of the Milky Way environment and in the final properties of the MW at $z = 0$ and, in particular, of the most metal-poor stars observed in the Galactic halo.

In Figure 8 we show the redshift evolution of the MWenv metallicity Z_{MWenv} ⁸ predicted by GAMESH (solid black line) and the corresponding values obtained by assuming instant reionisation (dotted red line). As already noted commenting Figure 4 and 5, the star-formation history of Pop III stars is remarkably different when an accurate model for the radiative feedback is taken into account and their rapid burst, predicted by our simulation, is clearly imprinted in the metallicity of the diffuse, external medium. In fact, Z_{MWenv} experiences a rapid increase at high redshift, reaching the critical value $Z_{cr} = 10^{-4} Z_{\odot}$ already at $z \sim 14$.

⁸ This value is defined as the metallicity of the medium surrounding the collapsed halos and it is calculated as ratio of the mass of metals over the total mass of the gas.

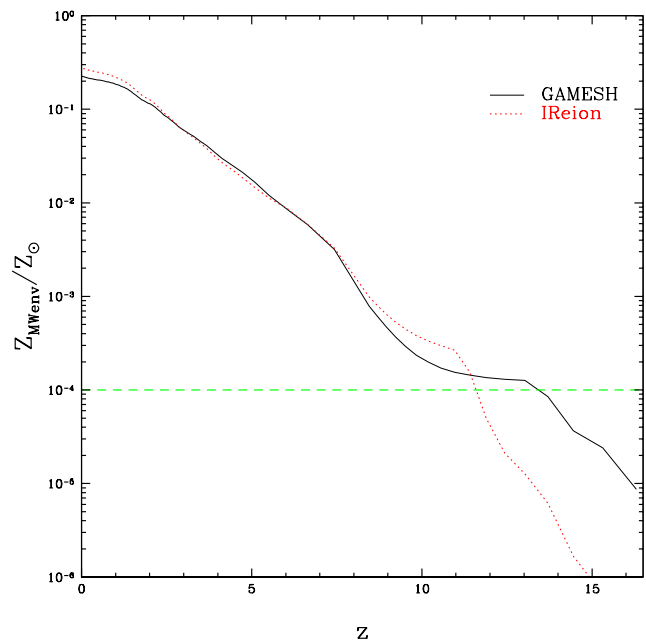


Figure 8. Evolution in redshift of the Milky Way environment metallicity Z_{MWenv} (solid black line) in solar metallicity units. The values obtained by assuming instant reionisation are shown in dotted red line. The green dashed line shows, as reference, the value adopted for the critical metallicity to form Pop II stars.

After a flat evolution corresponding to the Pop III to Pop II transition the increasing trend is restored by the increase in SFR of Pop II stars. As for the SFR (see Figure 4), Z_{MWenv} becomes consistent with the value predicted by the IReion case in the redshift interval $3 < z \leq 8$ after which it flattens. Note that a 15% difference in the SFR at $z = 0$ due to an extended reionisation is reflected in 25% decrease of the final metallicity Z_{MWenv} .

It should be noted that the trend at high redshift is

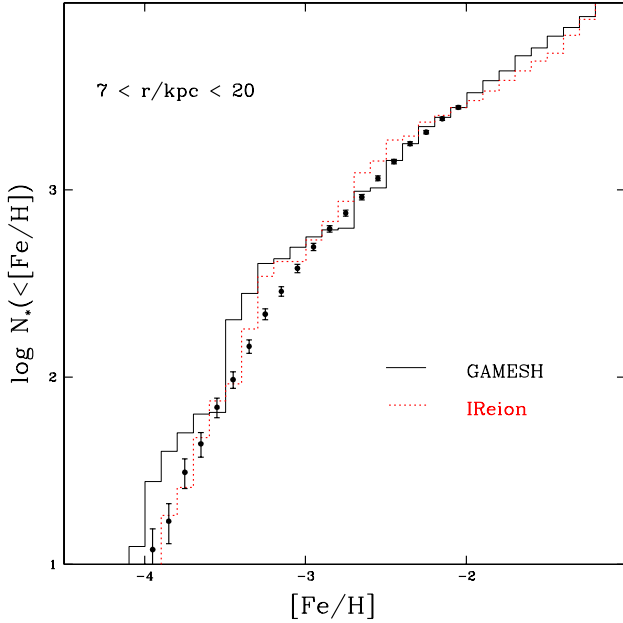


Figure 9. MDF of the central galaxy calculated by **GAMESH** (solid black line) and in the **IReion** case (dotted red line) in the radial range $7 < r < 20$ kpc. Black points indicate observed data taken from Beers & Christlieb 2005.

certainly un-physical because the metallicity of the medium surrounding the galaxies on our box scale is expected to increase more progressively in redshift from very low Z_{MWenv} as correctly predicted by the **IReion** model. We thoroughly investigated what causes this trend, finding a concurrence of reasons. First, our N-body simulation does not provide a sufficient mass resolution to accurately predict the distribution of low mass mini-halos, which are expected to have played a relevant role in the early metal enrichment of the MW and its dwarf satellites (see for example Salvadori & Ferrara 2009; Sales et al. 2014; Salvadori et al. 2014). As a consequence **GAMESH** tends to over-estimate the production/dispersion of metals in the first star-forming objects. Second, as indicated by pure semi-analytic calculations that simultaneously reproduce different data-sets at $z = 0$ (see Salvadori & Ferrara (2012); Salvadori et al. (2014)), a better description of both the stellar life-times and the inhomogeneous dispersion of metals into the $MWenv$ is required when the effect of an in-homogeneous reionisation are considered. Finally, on the radiative feedback side, the extension of the frequency range to a Lyman-Werner frequency band is necessary to correctly reproduce the star formation in H_2 -cooling halos.

The Metallicity Distribution Function (MDF) of ancient stars in the final MW-like galaxy, clearly reflects the different evolution of both the total SFR and Z_{MWenv} at $z > 8 - 10$, where the majority of $[Fe/H] < -3$ stars are formed (de Bressan et al. 2014). In Figure 9 we compare the MDFs of $z = 0$ stars in the radial range $1 \text{ kpc} < r < 20$ kpc for the **IReion** and **GAMESH** runs. Black points with errorbars show the available data for Galactic halo stars in the same Galactocentric ranges (see also SF10).

Both curves show a satisfactory agreement in the over-

all trend of the observed data, and the differences between the two runs are much smaller than the errors induced when considering different MW merger histories (Salvadori, Schneider & Ferrara 2007; de Bressan et al. 2014). While the **GAMESH** run fits the data for $[Fe/H] > -3$ (see Beers & Christlieb 2005), it clearly overproduces the number of low-metallicity stars, $[Fe/H] < -3$. This is due to the slower progress of metal enrichment, as reflected by the shallow increase of Z_{MWenv} in the redshift range $8 < z < 13$ (see the plateau in Figure 8). We interpret this issue as a clear indication that the current resolution of the simulation does not allow to accurately trace star formation and radiative feedback at the highest redshifts.

5 CONCLUSIONS

In this work we investigated the early formation process of a MW-like galaxy by using **GAMESH**, a novel tool combining for the first time in the literature, a N-body simulation with a detailed chemical and radiative feedback in a self-consistent framework. Many aspects of the formation process have been discussed along the cosmic time as the evolution of the SFR, the Pop III to Pop II transition, the statistics of progenitor halos in which star formation is suppressed, and finally the interplay between chemical and radiative feedback in setting up the chemical properties of the Local Group and the final MDF of the Galactic halo.

Even with a low resolution N-body simulation, which lacks in statistics and does not allow to draw definite conclusions on many aspects of the problem, **GAMESH** has been proven to be an ideal tool to provide both a comprehensive vision of the early formation of the Galaxy and its reionisation process, and to include an accurate self-consistent treatment of chemical, mechanical and radiative feedback in numerical simulations.

The capability of **GAMESH** to switch between pure semi-analytic treatment and inclusion of accurate RT enabled us to carefully compare and contrast all the results obtained by both models and to compare with observed properties of the Galaxy and the surrounding environment at $z = 0$. In addition, the **GAMESH** algorithm is very general and does not limit its field of applicability to a Milky Way formation process; it can be extended and adapted to a wide range of galaxy and star formation related topics.

A future work, based on high mass and spatial resolution simulation, is certainly needed to establish with accuracy the epoch and extension of reionisation and its interplay with chemical feedback, the role of mini-halos and finally the signatures of global feedback processes on the stellar halo MDF and luminosity function of MW satellites.

ACKNOWLEDGMENTS

The authors would like to thank the anonymous referee for his very constructive comments. L.G. thanks R. Valiante for the invaluable support during the GAMETE refactoring and re-engineering. S. Salvadori acknowledges support from the Netherlands Organisation for Scientific Research (NWO), VENI grant 639.041.233. R.S., A.M. and S.S. wish to thank

the Osservatorio Astrofisico di Arcetri where the project was originally conceived and developed in successive meetings.

The authors acknowledge Andrea Ferrara and Benedetta Ciardi for their very constructive comments. We also thank the 4C Institute at the Scuola Normale Superiore of Pisa for the computational resources necessary to develop and test GAMESH. We also acknowledge PRACE⁹ for awarding us access to the CEA HPC facility "CURIE@GENCI"¹⁰ with the Type B project: High Performance release of the GAMESH pipeline.

The research leading to these results has received funding from the European Research Council under the European Union's Seventh Framework Programme (FP/2007-2013) / ERC Grant Agreement n. 306476.

REFERENCES

- Alvarez M. A., Busha M., Abel T., Wechsler R. H., 2009, *ApJ Letters*, 703, L167
- Barkana R., Loeb A., 2001, *PhysRep*, 349, 125
- Battaglia G. et al., 2005, *MNRAS*, 364, 433
- Beers T. C., Christlieb N., 2005, *ARAA*, 43, 531
- Belokurov V. et al., 2006, *ApJ Letters*, 647, L111
- Benson A. J., Frenk C. S., Lacey C. G., Baugh C. M., Cole S., 2002a, *MNRAS*, 333, 177
- Benson A. J., Lacey C. G., Baugh C. M., Cole S., Frenk C. S., 2002b, *MNRAS*, 333, 156
- Bovill M. S., Ricotti M., 2009, *ApJ*, 693, 1859
- Bovill M. S., Ricotti M., 2011a, *ApJ*, 741, 17
- Bovill M. S., Ricotti M., 2011b, *ApJ*, 741, 18
- Boylan-Kolchin M., Bullock J. S., Kaplinghat M., 2012, *MNRAS*, 422, 1203
- Brook C. B., Kawata D., Scannapieco E., Martel H., Gibson B. K., 2007, *ApJ*, 661, 10
- Brown T. M. et al., 2012, *ApJ Letters*, 753, L21
- Bruzual A. G., Charlot S., 1993, *ApJ*, 405, 538
- Busha M. T., Alvarez M. A., Wechsler R. H., Abel T., Strigari L. E., 2010, *ApJ*, 710, 408
- Chomiuk L., Povich M. S., 2011, *AJ*, 142, 197
- Ciardi B., Ferrara A., Marri S., Raimondo G., 2001, *MNRAS*, 324, 381
- Couchman H. M. P., Rees M. J., 1986, *MNRAS*, 221, 53
- de Bressan M., Schneider R., Valiante R., Salvadori S., 2014, *MNRAS*, 445, 3039
- Dijkstra M., Haiman Z., Rees M. J., Weinberg D. H., 2004, *ApJ*, 601, 666
- D'Onghia E., Besla G., Cox T. J., Hernquist L., 2009, *NATURE*, 460, 605
- D'Onghia E., Springel V., Hernquist L., Keres D., 2010, *ApJ*, 709, 1138
- Efstathiou G., 1992, *MNRAS*, 256, 43P
- Gnedin N. Y., 2000, *ApJ*, 542, 535
- Graziani L., Maselli A., Ciardi B., 2013, *MNRAS*, 431, 722
- Haardt F., Madau P., 2012, *ApJ*, 746, 125
- Hoeft M., Yepes G., Gottlöber S., Springel V., 2006, *MNRAS*, 371, 401
- Kawata D., Gibson B. K., 2003a, *MNRAS*, 340, 908
- Kawata D., Gibson B. K., 2003b, *MNRAS*, 346, 135
- Kitayama T., Tajiri Y., Umemura M., Susa H., Ikeuchi S., 2000, *MNRAS*, 315, L1
- Klypin A., Kravtsov A. V., Valenzuela O., Prada F., 1999, *ApJ*, 522, 82
- Koposov S. E., Yoo J., Rix H.-W., Weinberg D. H., Macciò A. V., Escudé J. M., 2009, *ApJ*, 696, 2179
- Kravtsov A. V., Gnedin O. Y., Klypin A. A., 2004, *ApJ*, 609, 482
- Li T. Y., Alvarez M. A., Wechsler R. H., Abel T., 2014, *ApJ*, 785, 134
- Li Y.-S., De Lucia G., Helmi A., 2010, *MNRAS*, 401, 2036
- Lunnan R., Vogelsberger M., Frebel A., Hernquist L., Lidz A., Boylan-Kolchin M., 2012, *ApJ*, 746, 109
- Macciò A. V., Kang X., Fontanot F., Somerville R. S., Koposov S., Monaco P., 2010, *MNRAS*, 402, 1995
- Madau P., Kuhlen M., Diemand J., Moore B., Zemp M., Potter D., Stadel J., 2008, *ApJ Letters*, 689, L41
- Maselli A., Ciardi B., Kanekar A., 2009, *MNRAS*, 393, 171
- Maselli A., Ferrara A., 2005, *MNRAS*, 364, 1429
- Maselli A., Ferrara A., Ciardi B., 2003, *MNRAS*, 345, 379
- Milosavljević M., Bromm V., 2014, *MNRAS*, 440, 50
- Moore B., Ghigna S., Governato F., Lake G., Quinn T., Stadel J., Tozzi P., 1999, *ApJ Letters*, 524, L19
- Muñoz J. A., Madau P., Loeb A., Diemand J., 2009, *MNRAS*, 400, 1593
- Noh Y., McQuinn M., 2014, *MNRAS*, 444, 503
- Ocvirk P. et al., 2014, *ApJ*, 794, 20
- Okamoto T., Gao L., Theuns T., 2008, *MNRAS*, 390, 920
- Sales L. V., Marinacci F., Springel V., Petkova M., 2014, *MNRAS*, 439, 2990
- Salvadori S., Ferrara A., 2009, *MNRAS*, 395, L6
- Salvadori S., Ferrara A., 2012, *MNRAS*, 421, L29
- Salvadori S., Ferrara A., Schneider R., 2008, *MNRAS*, 386, 348
- Salvadori S., Ferrara A., Schneider R., Scannapieco E., Kawata D., 2010, *MNRAS*, 401, L5
- Salvadori S., Schneider R., Ferrara A., 2007, *MNRAS*, 381, 647
- Salvadori S., Tolstoy E., Ferrara A., Zaroubi S., 2014, *MNRAS*, 437, L26
- Sawala T. et al., 2014, *arxiv:1406.6362*
- Scannapieco E., Kawata D., Brook C. B., Schneider R., Ferrara A., Gibson B. K., 2006, *ApJ Letters*, 653, 285
- Schaerer D., 2002, *A&A*, 382, 28
- Schneider R., Ferrara A., Natarajan P., Omukai K., 2002, *ApJ*, 571, 30
- Schneider R., Omukai K., Inoue A. K., Ferrara A., 2006, *MNRAS*, 369, 1437
- Sobacchi E., Mesinger A., 2013, *MNRAS*, 432, L51
- Somerville R. S., 2002, *ApJ Letters*, 572, L23
- Springel V. et al., 2008, *MNRAS*, 391, 1685
- Thoul A. A., Weinberg D. H., 1996, *ApJ*, 465, 608
- Tinsley B. M., 1980, *Fundamentals of Cosmic Physics*, 5, 287
- Willman B. et al., 2005, *AJ*, 129, 2692
- Zahn O., Mesinger A., McQuinn M., Trac H., Cen R., Hernquist L. E., 2011, *MNRAS*, 414, 727
- Zucker D. B. et al., 2006a, *ApJ Letters*, 650, L41
- Zucker D. B. et al., 2006b, *ApJ Letters*, 643, L103

⁹ <http://www.prace-ri.eu/>

¹⁰ <http://www-hpc.cea.fr/en/complexe/tgcc-curie.htm>